Molecular Vision 2018; 24:902-912 <http://www.molvis.org/molvis/v24/902>
Received 21 September 2018 | Accepted 31 December 2018 | Published 31 December 2018

Micromorphology analysis of the anterior human lens capsule

Ştefan Ţălu,[1] Vivian M. Sueiras,[2] Vincent T. Moy,[3] Noël M Ziebarth[2,3]

(The first two authors contributed equally to this work.)

[1]The Technical University of Cluj-Napoca, The Directorate of Research, Development and Innovation Management (DMCDI), Cluj-Napoca, Romania; [2]Department of Biomedical Engineering, University of Miami College of Engineering, Coral Gables, FL; [3]Department of Physiology and Biophysics, University of Miami Miller School of Medicine, Miami, FL

Purpose: This study aimed to quantify the three-dimensional micromorphology of the surface of the human lens capsule as a function of age.

Methods: Imaging experiments were conducted on whole human lenses received from eight human cadavers (donor age range: 30–88 years). Imaging was performed with an atomic force microscope (AFM) in contact mode in fluid. The porosity and surface roughness were quantified from the height images obtained. A novel approach, based on stereometric and fractal analysis of three-dimensional surfaces developed for use in conjunction with AFM data, was also used to analyze the surface microtexture as a function of age.

Results: The AFM images obtained depict a highly ordered fibrous structure at the surface of the lens capsule, although the overall structure visually changes with age. Porosity and roughness were quantified for each image and analyzed as a function of donor age. The interfibrillar spacing revealed an increasing trend with age, although this result was not significant ($p = 0.110$). The root mean square (RMS) deviation and average deviation significantly decreased with increasing age ($p<0.001$ for both). The fractal analysis provided quantitative values for 29 amplitude, hybrid, functional, and spatial parameters. All the hybrid parameters decreased with age, although not significantly. Of the functional parameters, the surface bearing index increased significantly with age ($p = 0.017$) and the summit height exhibited a decreasing trend with age ($p = 0.298$). Of the spatial parameters, the dominant radial wavelength trend moved toward an increase with age ($p = 0.103$) and the cross-hatch angle tended toward a decrease with age ($p = 0.213$).

Conclusions: Significant changes in the three-dimensional surface microtexture of the human lens capsule were found with age, although more experiments on a larger dataset are needed to conclude this with certainty. The analyzed AFM images demonstrate a fractal nature of the surface, which is not considered in classical surface statistical parameters. The surface fractal dimension may be useful in ophthalmology for quantifying human lens architectural changes associated with different disease states to further our understanding of disease evolution.

The lens capsule is an acellular basement membrane completely encapsulating the lens of the eye. It functions as a medium of biochemical interchange [1], allowing for the passive exchange of metabolic substrates and waste between the ocular environment and the lens cells [2,3]. Since no evidence has been found for pores in the lens capsule, all molecules must passively diffuse through the interwoven fibrous network that forms the lens capsule. This network has been imaged previously using cryoelectron microscopy [4,5], scanning helium ion microscopy [3], and atomic force microscopy (AFM) [6-10]. However, there are no studies that quantify the structure of the human anterior lens capsule as a function of age.

AFM is an especially advantageous technique for imaging the lens capsule, since it can produce high-resolution images of the topography of the surface without altering the natural state of the sample and maintaining hydration [11]. In addition, because the cantilever moves in contact with the sample topography, quantitative information regarding the surface roughness and porosity can be obtained. Recent advances in computational software technology can provide further analysis of the surface using a statistical and fractal/multifractal geometry approach. Such an approach is well suited for biological structures, such as the lens capsule, which can be characterized by multiple levels of substructure comprising the same general pattern iterated in an ever-decreasing cascade [12-19]. When investigating small details of the surface structure at different scales, the self-similar fractal will reveal an overall pattern of repeated elements. Since these repeated elements are seen at all levels of magnification, the fractal is considered an infinitely complex pattern [18].

An advanced, quantitative description of the microstructure and surface topography of the lens capsule may provide a better understanding of the relationship between the surface

Correspondence to: Noël M. Ziebarth, Department of Biomedical Engineering University of Miami College of Engineering, 1251 Memorial Drive, MEA 219 Coral Gables, FL 33146; Phone +1 (305) 284-4520; FAX: +1 (305) 284-6494; email: nziebarth@miami.edu

topography, microstructure, and biophysical–chemical properties. The lens capsule serves as a semipermeable membrane that allows nutrients and antioxidants to pass through it and enter the lens. Therefore, any modifications to this structure with age could affect diffusion into the lens. Changes to the normal diffusion patterns of molecules relevant to lens biology may affect its ability to function normally. The purpose of the current study was quantifying the anterior lens capsule structure as a function of age using advanced image processing techniques based on a multifractal geometry approach.

METHODS

Tissue preparation protocol: Whole lenses were received from eight human cadavers (donor age range: 30–88 years). The donor eyes, obtained from the Florida Lions Eye Bank (Miami, FL), were transported to the laboratory in sealed containers and stored at 4 °C before use. All human eyes were obtained and used in compliance with the guidelines of the Declaration of Helsinki for research involving the use of human tissue. The lenses were removed from the whole globes and placed in Dulbecco's Modified Eagle's Medium (DMEM, D1145, Sigma-Aldrich, St. Louis, MO) until they could be further prepared for imaging. DMEM has been shown to be effective at maintaining lens hydration levels without causing capsular delamination [20]. The lenses were visually examined before imaging, and no abnormalities other than various degrees of age-related nuclear cataract were observed. Since only donor age and cause of death were provided, it is unknown whether the donor had any diseases that could affect the lens structure. To stabilize the lens for imaging, the posterior half of the whole lens was embedded with a 5% agarose gel (weight/volume in deionized water, A0169–100G, Sigma-Aldrich, St. Louis, MO). Here, agarose powder was amalgamated with deionized water to form a gel in which the lens was embedded. Lenses were placed anterior side up, with only the posterior half of the lens submerged, before the gel hardened. The Petri dish was then filled with DMEM to the point where the exposed portion of the embedded lens was fully submerged to prevent dehydration. With this sample preparation technique, the anterior surface of the lens, corresponding to the anterior lens capsule, was exposed and could be successfully imaged.

Atomic force microscopy: Imaging of the anterior lens capsule was accomplished with a MFP-3D-BIO AFM (Oxford Instruments, Santa Barbara, CA) by situating the cantilever tip (20-nm tip radius, 0.01 N/m nominal spring constant, MLCT series, Bruker AFM Probes, Camarillo, CA) on the anterior apex of the lens. AFM images of the anterior surface of the lens, corresponding to the lens capsule, were then obtained under fluid in contact mode, in which the cantilever tip is held in constant contact with the sample surface, maintaining constant cantilever deflection while scanning. Height and deflection images were captured at multiple scan lengths for all the lens samples. All images were acquired at scan rates ranging from 0.25 Hz to 0.75 Hz with at least 256 × 256 pixel image resolution. The images acquired were within a region in the central apex of the anterior lens capsule of approximately 100 × 100 µm.

Image postprocessing: All images obtained were processed using the software integrated with the MFP-3D-BIO AFM. The height data used to reconstruct the images were obtained from the Z sensor signal channel. The height data collected from the "height" signal is not accurate when sample features are greater than 0.1 µm, as is the case for whole lenses. Since the Z sensor signal is obtained from the linear variable differential transformers position sensors attached to the piezo stacks, this signal corresponds to the true topography of the sample surface. To compensate for the natural curvature of the lens, all the data acquired were flattened using an x-y plane fit, as well as a flatten order 1. This "Flatten Image" command fits each scan line with a polynomial line and subtracts it from the data. In addition, a 3 × 1 median filter was applied to the images after flattening. The edges of the scan, where the piezoelectric actuator was out of range of the sample height (pure white or pure black image), were not included in the analysis. Care was also taken to minimize the inclusion of motion artifacts, which are common at the end of image acquisition.

Image analysis: For each AFM image, the height of the cantilever as it moves across the topography of the lens capsule surface was recorded. This quantitative information can be extracted and analyzed. In this study, the interfibrillar spacing was calculated from the peak-to-peak distances along one representative line of data using OriginLab (Northampton, MA). The fiber dimensions were defined as the full width at half maximum of the peaks along the line of data. Four quantitative parameters were also calculated using the software integrated with the MFP-3D-BIO to characterize the roughness of the lens capsule surface, as follows: root-mean-square (RMS) deviation, average deviation, skewness (asymmetry around the mean), and kurtosis (peakedness or flatness compared with the normal distribution). These values were calculated for each Z sensor image.

One representative 5 × 5 µm height image was selected per donor for further three-dimensional surface texture characterization. The 5 × 5 µm height image acquired was converted into an uncompressed linear eight-bit gray scale

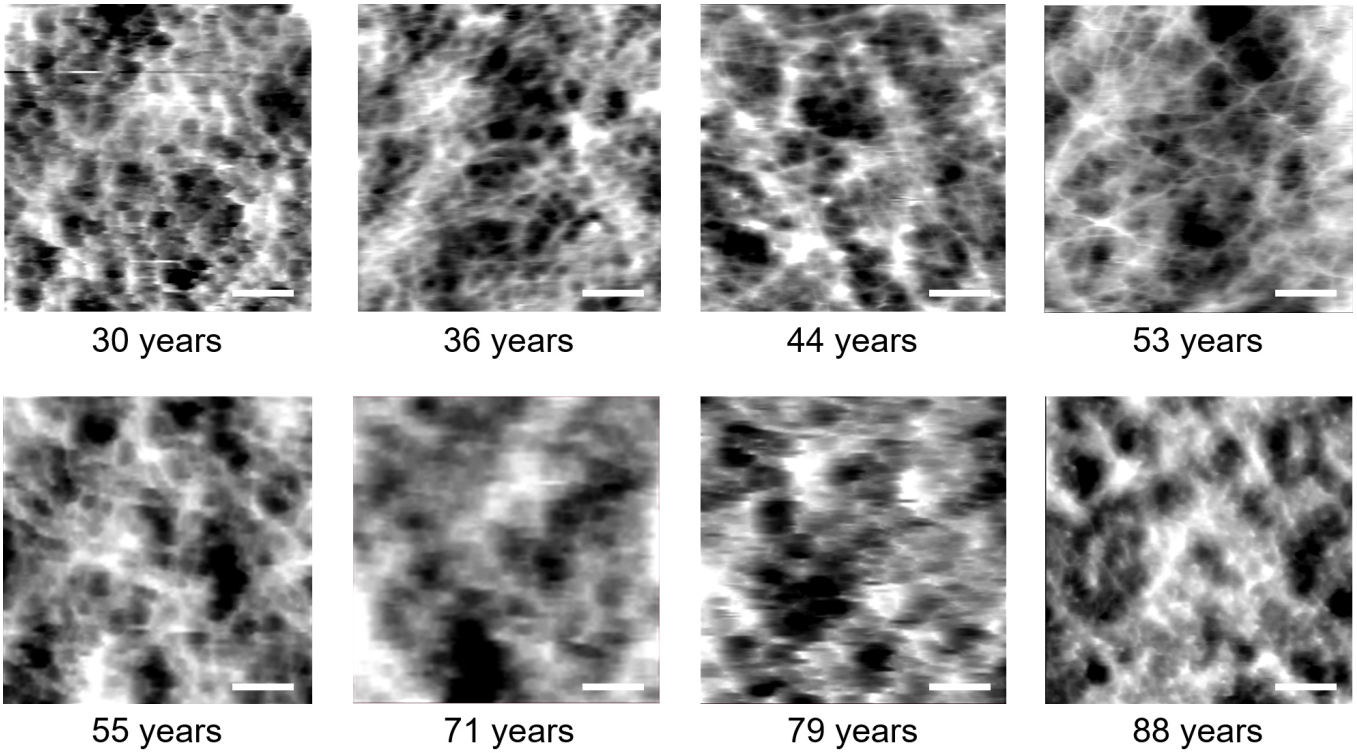

Figure 1. Atomic force microscopy (AFM) images of the human lens capsule surfaces from the eight human donors. All images' dimensions are 5 × 5 µm and were obtained from the Z sensor channel. The scale bar represents 1 µm.

tagged image format (TIF). A novel fractal analysis technique was applied to the images. The fractal analysis produced graphs of the height distribution histogram, Abbott–Firestone curve, and angular spectrum, which are microtexture fractal parameters that can quantify the basic geometry of the lens capsule's texture. The fractal dimension value was also determined for each sample. Additional roughness analysis was performed on the TIF images using Scanning Probe Image Processor (SPIP™) software (Image Metrology, Denmark). This analysis produced an additional twenty-nine quantitative roughness parameters that can be divided into amplitude, hybrid, functional, and spatial parameters.

RESULTS

The height images obtained from the Z sensor signal after postprocessing are shown in Figure 1 from all eight samples used in this study. These images depict the vertical displacement of the cantilever tip as it is scanned across the topography of the sample. The images portray a highly ordered structure at the anterior surface of the central apex of the human lens capsule for all ages. From Figure 1, it can also be seen that the geometric characteristics of the anterior human lens capsule, as well as configurations of the whole patterns, change in both size and form with age.

Each image obtained underwent a quantitative analysis to determine the porosity and roughness of the specimen. The average interfibrillar spacing and fiber diameter dimensions for the 8 samples were 0.81 ± 0.35 µm and 282 ± 111 nm, respectively. When analyzed as a function of age, the interfibrillar spacing revealed an increasing linear trend, although this was not significant (p = 0.110). This increase in interfibrillar spacing signifies that the characteristic honeycomb structure of the anterior lens capsule becomes less compact with age. There was no relationship between fiber diameter and age. When determining the roughness parameters, one sample (age 79) produced data more than two standard deviations from the mean, thus, it was considered an outlier and excluded from the final roughness analysis. The average RMS deviation, average deviation, skewness, and kurtosis parameters for the seven analyzed samples were 20.05 ± 4.20 nm, 15.75 ± 3.25 nm, 0.01 ± 0.12, and 0.21 ± 0.17, respectively. Of the four roughness parameters that were determined, the RMS deviation and average deviation revealed a linear relationship with age. Both RMS and average deviation values significantly decreased with increasing age (p<0.0001

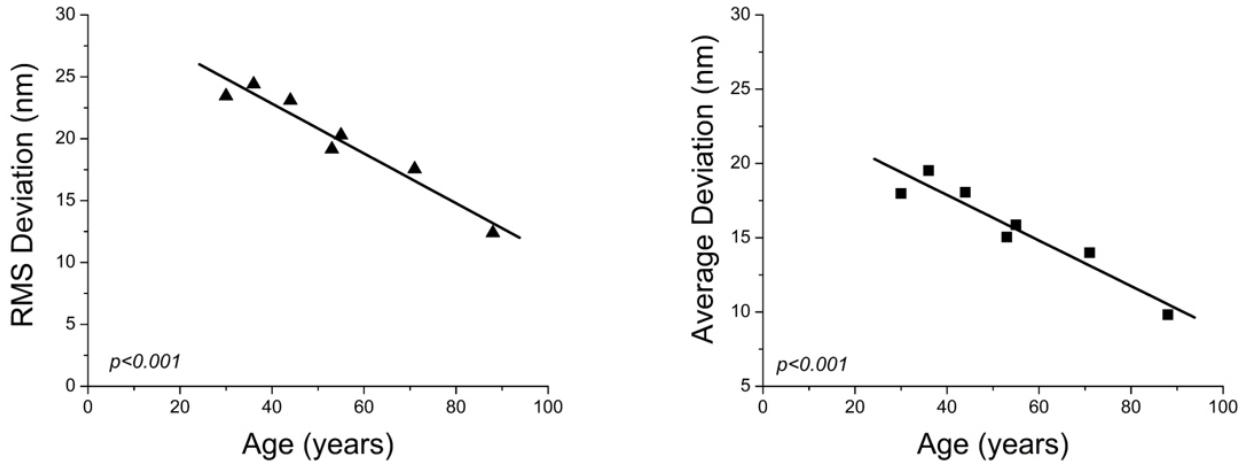

Figure 2. Root mean square (RMS) and average deviation roughness as a function of age. The surface of the human lens capsule becomes significantly smoother with age.

for both), meaning that the anterior lens capsule becomes smoother with age. The porosity and roughness parameters are summarized in Table 1. The roughness data as a function of age are shown in Figure 2.

From the fractal analysis, the height distribution within each image was measured and integrated (Figure 3). This histogram provides the density of the distribution of the data points on the surface as a percentage of the entire population of data point measurements. It was constructed by plotting the fraction of surface heights lying between two specific heights as a function of height. As would be expected, the peak of the histogram was at zero for all the samples, which represents the middle plane of the anterior lens capsule surface that was imaged. Moving farther away from the central imaged plane along the axis, there was less coverage (more empty space). When reviewing all the collected data, in this study, a slight pattern emerged in relation to age. The height distributions for the samples of ages 30, 36, and 44 years depicted a smoother transition in the histogram versus the peakedness that started to be seen in the 53-year-old and became more prominent in the older lenses. For most of the older lenses, the histogram revealed a broader spread, with an increased percentage of the collected data points within the depth extremes. This can be confirmed in the observable decrease of their histogram integration curve slopes. These trends in the histogram are most likely because the lens capsule structure becomes less compact with age; thus, the AFM tip can collect data at a lower plane in these void areas, causing a spread in the height histogram.

The Abbott–Firestone curve, or bearing area curve, was obtained for each sample by inverting the profile trace of the cumulative height distribution histogram (Figure 4). The bearing area curve quantifies the contact area; for a surface that bears load, a larger contact area would be indicative of enhanced load-bearing capabilities. A primary purpose of the lens capsule is to maintain the structural integrity of the lens fiber cells; therefore, its load bearing capability is of great importance. Although the slope of the bearing ratio curves for each image differs, signifying a variability in the coverage area of the capsule structure, there does not seem to be a relationship with age. Therefore, the load bearing capability of the anterior lens capsule appears to be consistent with age.

To analyze whether the sample's topography exhibits any dominant directional patterns, an angular spectrum for each sample was generated (Figure 5). The angular spectrum displays the direction of the sample's texture as an angular

Table 1. Summary of quantitative roughness and porosity parameters obtained from the images of the human lens capsules.

Interfibrillar spacing (µm)	Fiber diameter (nm)	RMS deviation (nm)	Average deviation (nm)	Skewness (no unit)	Kurtosis (no unit)
0.82±0.35	282±111	20.05±4.20	15.75±3.25	0.01±0.12	0.21±0.17

plot. Any peaks in the graph are indicative of a dominant directional alignment of the capsule's structure. For the angular spectrum, the relative amplitudes (horizontal axis) for the various angles were determined by the summation of the amplitudes along equiangular-separated radial lines. The consistency of the distribution of the data across the angular dimension signifies that the anterior lens capsule surface is isotropic in the x-y plane. There was no significant relationship of the angular spectrum with respect to age.

The fractal dimension of each sample was determined through the analysis of the Fourier amplitude spectrum. This spectrum was generated by extracting the amplitude Fourier profile for different angles and then calculating the logarithm of their frequency and amplitude coordinates. The fractal dimension (D) for each direction was calculated as:

$$D = \frac{(6+s)}{2}$$

where *s* is the negative slope of the log-log curves. The fractal dimension for the sample (Table 2), as a whole, was determined by averaging the fractal dimensions for all directions. Although there does not appear to be a linear correlation between the calculated fractal dimension and age, if one were to group the samples by relative age groups (younger <55, older ≥55), the older lens capsules would display an increased fractal dimension, signifying an increased complexity and disorganization of the surface structure with age. The disorganization of the surface can be seen qualitatively with increasing age in Figure 1. For the AFM image of the human lens capsules analyzed, a statistically significant difference from a flat surface (p<0.05) was found for all values of the fractal dimension.

Several additional quantitative roughness parameters were analyzed to provide complementary information to the roughness parameters analyzed using the software incorporated with the MFP-3D AFM system (Table 3). The hybrid roughness parameters, reflecting the slope gradients and their calculations, are based on local slopes in the height direction (z-axis). Therefore, these parameters are directly related to surface roughness. Four of these hybrid parameters showed a decreasing trend with age, as follows: mean summit curvature (S_{sc}), RMS gradient (S_{dq}), area RMS slope (S_{dq6}), and surface area ratio (S_{dr}). S_{sc} is the average of the principal curvature of the local maximums on the surface. S_{dq} is the RMS value of

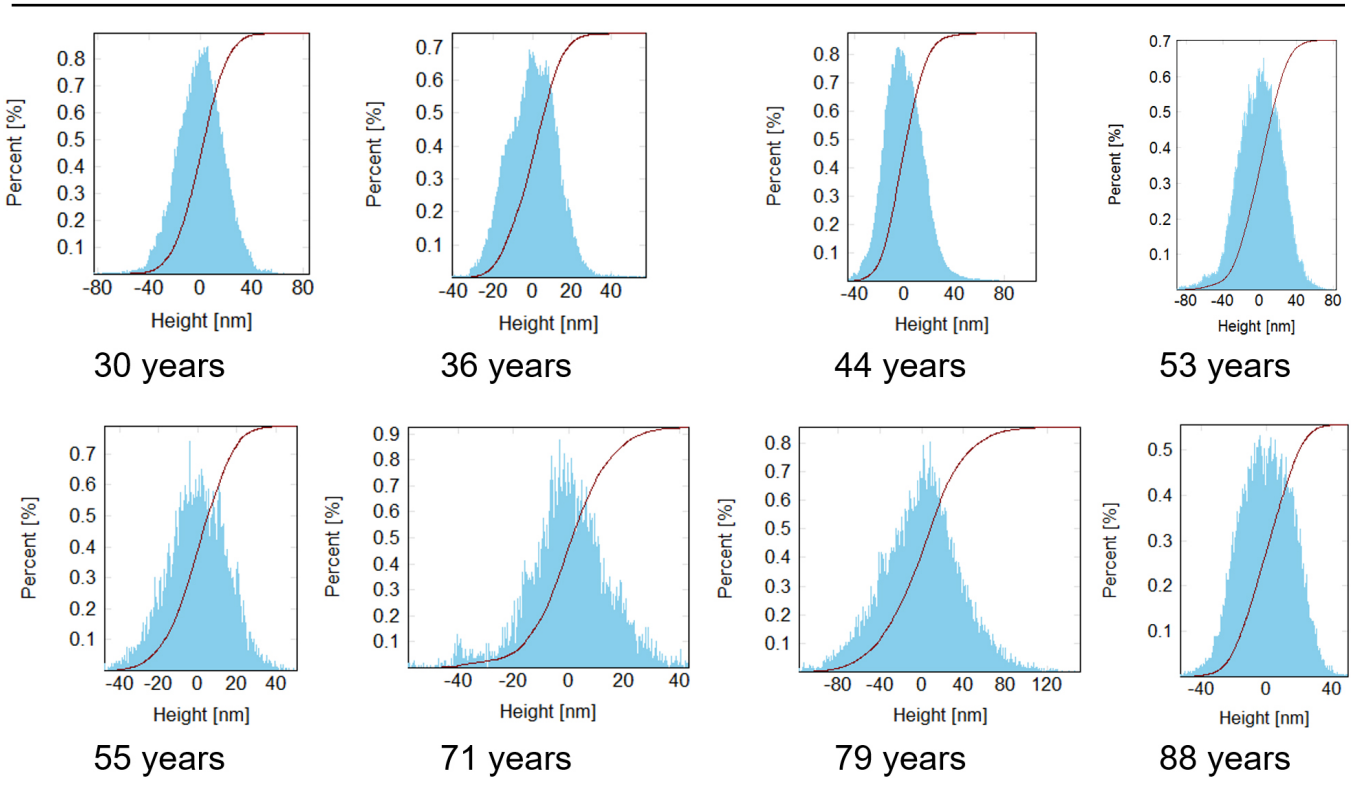

Figure 3. Height distribution histograms with integration curve of the histogram for the atomic force microscopy (AFM) images of the surfaces of the eight human lens capsules. The horizontal axis is graduated in depth, while the vertical axis is graduated in percentage of the whole population of data.

the surface slope within the sampling area. S_{dq6} is similar to the RMS gradient, but it includes more neighbor pixels in the calculation of the slope for each pixel. Finally, S_{dr} expresses the increment of the interfacial surface area relative to the area of the projected (flat) x-y plane. All four of these parameters are slightly different methods of quantifying surface roughness; a decreasing trend with age is consistent with the other measures of surface roughness (Figure 2).

The functional parameters were defined from the Abbott–Firestone curve and used for characterizing bearing and fluid retention properties. Two of these functional parameters showed age-related trends: surface bearing index (S_{bi}) and reduced summit height (S_{pk}). S_{bi} significantly increased with age ($p = 0.017$). For a Gaussian height distribution, S_{bi} approaches 0.61 for increasing numbers of pixels. A larger number indicates a good bearing property, but it is also representative of wear. The increase in the surface bearing index with age indicates that the surface of the lens capsule shows evidence of wear, or erosion, with age. There was a decreasing trend in S_{pk} with age. S_{pk} is a measure of the peak height above the core roughness. A decreasing trend in this parameter coincides with the trend observed in RMS and average roughness: Roughness decreases with age. A reduction in S_{pk} is indicative of a smoother surface with age.

Of the spatial parameters quantified, the dominating radial wavelength (S_{rw}) and cross-hatch angle (S_{ch}) showed age-related trends. S_{rw} is the dominating wavelength found in the radial spectrum. S_{rw} increased with age, although not significantly ($p = 0.103$). S_{ch} is the angle difference between the two most dominant angles found in the image by analyzing its autocorrelation function. This angle decreased with age, although not significantly ($p = 0.213$). Both these trends demonstrate that the height transitions along the surface of the lens capsule are becoming more gradual with age. Once again, this result supports the claim that the lens capsule surface becomes smoother with age.

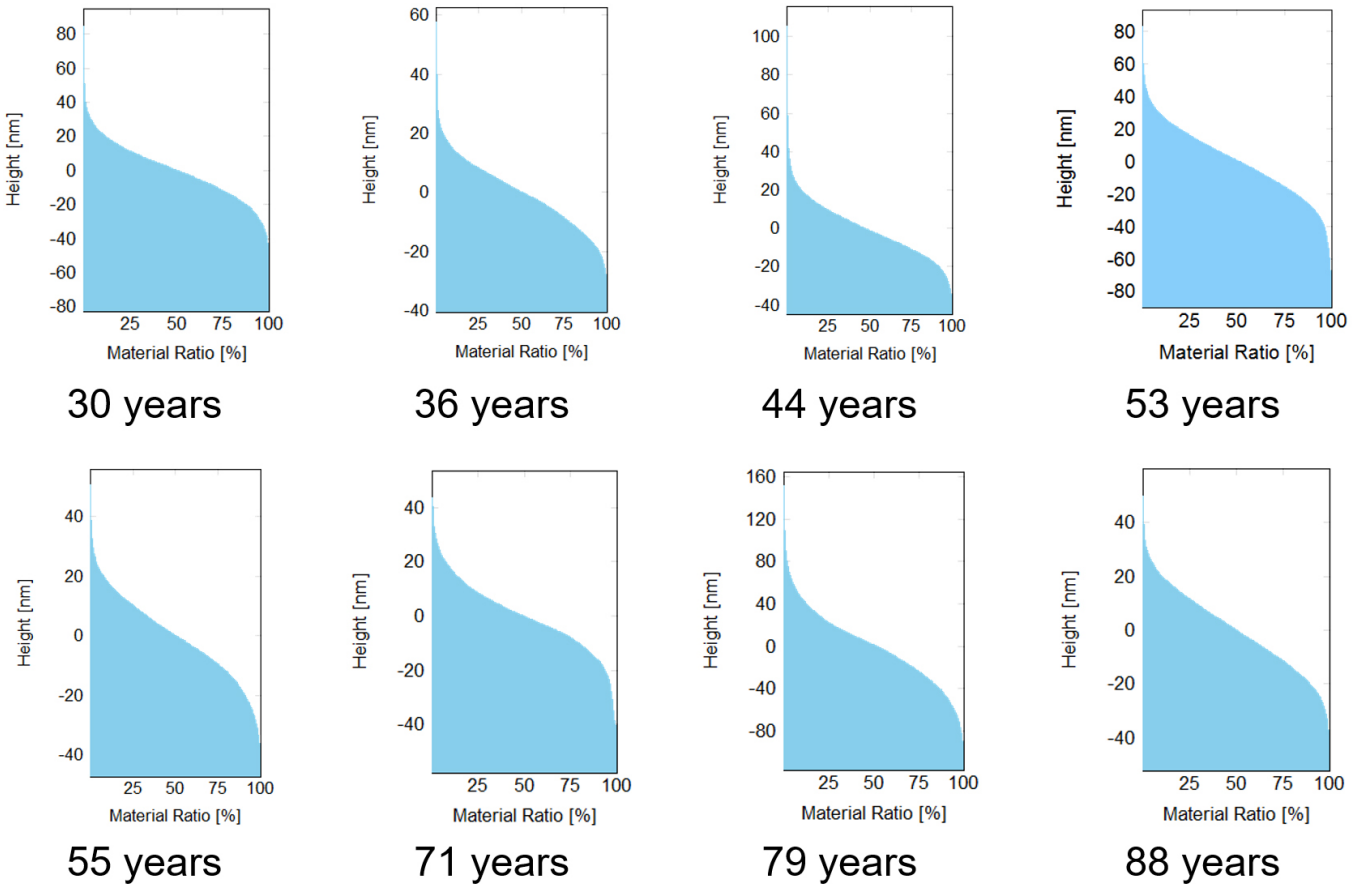

Figure 4. Abbott–Firestone curves for the atomic force microscopy (AFM) images of the surfaces of the eight human lens capsules. The curve represents the bearing ratio curve, which signifies the percentage of the material traversed in relation to the area of coverage. The vertical axis represents the measured heights and depths of the surface, and the horizontal axis depicts the bearing ratio in percentage.

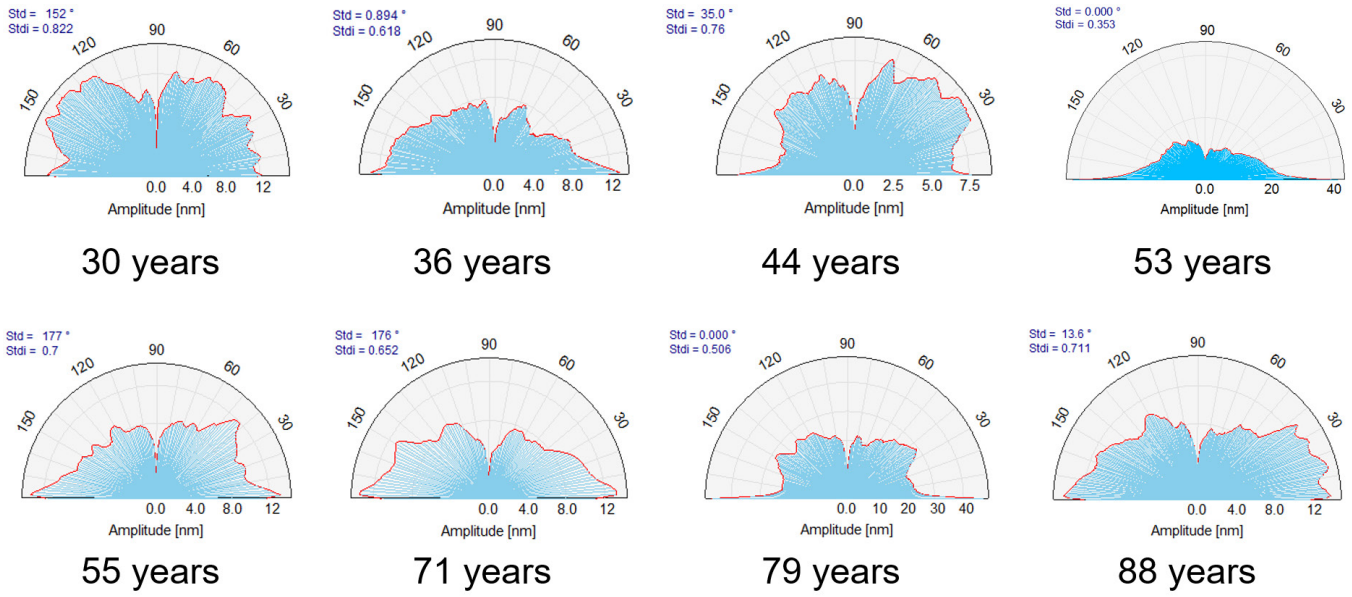

Figure 5. Angular spectrum of the samples' topography revealing the texture direction for the atomic force microscopy (AFM) images of the surfaces of the eight human lens capsules.

DISCUSSION

Images of the human lens capsule in situ were obtained using AFM. Maintaining the lens capsule in its natural, hydrated form allowed for the true topography of the capsule's surface to be captured. Since the lens capsule was sustained in its inherent tensile state, experienced natively when surrounding the lens, the anatomic features measured via AFM would be indicative of those present in vivo.

A visual assessment of the AFM height images (Figure 1) revealed a honeycomb structure, one that was especially prevalent in the younger lenses of 30 and 36 years of age, which demonstrated a highly organized structure. As the age of the human donor progressed, the topography of the capsule became more disorganized. The network took on an irregular appearance, and it became difficult to isolate the individual components. In addition, the AFM images of the younger lenses presented a consistently porous structure displaying more uniform interfibrillar dimensions at regular intervals. This contrasted with the older lenses, which exhibited a variable but larger pore structure at irregular intervals.

Further structural analysis of the obtained AFM images validated these visual observations. When comparing the interfibrillar spacing with age, an increasing trend emerged, although the fiber diameter showed no relationship with age. Furthermore, a roughness analysis of the images revealed a statistically significant decrease in topographical roughness with age. However, there did not appear to be asymmetric or peakedness variations related to age, as demonstrated by the skewness and kurtosis values, which did not exhibit a trend with age. These roughness results were validated by several

Table 2. The fractal dimension for the biologic nanostructures for each sample.

Donor Age (years)	Fractal dimension
30	2.11±0.01
36	2.08±0.01
44	2.03±0.01
53	2.04±0.01
55	2.20±0.01
71	2.16±0.01
79	2.15±0.01
88	2.12±0.01

additional hybrid parameters calculated using SPIP software. The hybrid parameters were calculated from the slope of the height of the data. Therefore, a decrease in these parameters was indicative of the height data being more consistent (lower slope), and by extension, less rough.

The fractal dimension, D, functions as a statistical means of quantitatively correlating the complexity of the capsule's structural components and the tissue as a whole [18]. A surface with increased complexity, possessing irregular shape, corresponds to an increased level of fractality and a larger fractal dimension. The results indicated that the fractal dimension for younger lens capsules was lower than the fractal dimension for older lens capsules. This validated what was observed visually in the images: The structure of the surface of the lens capsule became more disorganized with age, so it had a more irregular shape and increased complexity.

Both the qualitative and quantitative results demonstrated that the organization of the central anterior surface of the lens capsule changes with age. It is known from previous studies that the lens capsule comprises networks of laminin [21-25], collagen IV [21,26,27], entactin/nidogen [21,22,28], and some heparan sulfate proteoglycans, such as perlecan [21,29-31], collagen XVIII [32], collagen XV [33], and agrin [34]. The quantifiable increase in interfibrillar spacing, or porosity, with age may indicate a rearrangement of these various components in the network. Furthermore, since the lens capsule continuously thickens over time, this outermost layer of the capsule may experience increased tensile forces that would alter its pore structure. The decrease in roughness shown with the older lenses may also be explained by an increase in interfibrillar spacing since the height variability of the topography captured with the AFM would be more interspersed. Roughness is quantified digitally by the difference between black and white changes in the image. More pores, smaller in size, would result in many more transitions between black and white in the image, resulting in an increase in roughness. If the pore size increases with the older lenses, there would be fewer transitions between black and white, resulting in a decrease in the apparent roughness.

Located at the surface of the lens, the lens capsule is in direct contact with the intraocular fluids and is extremely susceptible to oxidative damage over time. In addition, the capsule is an acellular structure devoid of repair mechanisms, rendering it unable to recover from oxidative assault. There is extensive research on modifications to the internal lens structure and subsequent cataract formation due to oxidation [35-38]. Therefore, it is reasonable that the surface of the lens capsule would change with age, as indicated by the results of this study.

We previously published a study using AFM to image the anterior lens capsule in three different species, namely

Table 3. Select amplitude, hybrid, functional, and spatial roughness parameters obtained for the human lens capsule surface that show age-related trends.

Parameter	Units	Donor ages							
		30 years	36 years	44 years	53 years	55 years	71 years	79 years	88 years
Hybrid Parameters									
Mean Summit Curvature (S_{sc})	1/µm	12.99	8.92	20.22	19.14	2.81	1.59	16.90	5.50
Root mean square gradient (S_{dq})	None	0.32	0.16	0.23	0.26	0.12	0.08	0.43	0.15
Area Root Mean Square Slope (S_{dq6})	None	0.30	0.15	0.22	0.25	0.12	0.08	0.40	0.15
Surface area ratio (Sdr)	%	4.14	1.22	2.47	3.26	0.74	0.33	7.91	1.10
Functional Parameters									
Surface Bearing Index (S_{bi})	None	0.30	0.31	0.19	0.48	0.51	0.66	0.39	0.62
Reduced Summit Height (S_{pk})	nm	18.29	13.11	21.06	20.54	12.72	14.89	41.93	12.10
Spatial Parameters									
Dominant radial wavelength (S_{rw})	µm	2.69	3.09	3.25	5.01	1.89	5.08	5.09	5.04
Cross hatch angle (S_{ch})	degrees	104.70	35.78	28.36	106.80	43.73	21.00	70.86	17.64

the pig, cynomolgus monkey, and human [10]. No age-related trends were found with the human samples included in that study. The human and nonhuman primate data were grouped together to further investigate age-related trends, and a trend toward decreasing surface roughness with age was found. This result was confirmed with the current study: The surface roughness of the human anterior lens capsule significantly decreases with age. However, the previous study found a decrease in interfibrillar spacing with age when grouping the human and nonhuman primate samples. This result is the opposite of the trend we found in the current study; however, the previous trend observed was most likely skewed by the nonhuman primate samples. All four of these samples were from similarly aged, young monkeys, and the values obtained for interfibrillar spacing were similar to those obtained in the old human samples. It would be interesting to image aged monkey anterior lens capsules to see if the same trend observed in humans holds in nonhuman primates. It is likely that the trend will be the same, but that the starting point is higher in monkeys than it is in humans.

The lens is connected to the ciliary muscle via ligaments known as the zonule of Zinn. Previous studies have shown that the zonules connect physically to the lens capsule in the equatorially region of the lens. In the mouse lens, the zonules adhere to the surface of the capsule just anterior and posterior to the lens equator [39]. In the primate lens, studies have shown that the zonules penetrate into the lens capsule in this region [40]. In the current study, images were acquired of a region at the surface of the anterior pole of the lens. Therefore, the zonular attachment was not observed in any of the images acquired. It would be interesting to repeat this study in the peripheral region to observe any possible age-related changes in zonular attachment to the capsule. In addition, it can be expected that the composition of the lens capsule is not uniform throughout its surface, including an increased density of laminin in the periphery, which would most likely affect the structure observed via AFM.

Although the lens capsule samples imaged span a large age range (30–88 years), only one sample per age was imaged and several decades are only represented by one sample. The only information provided by the eyebank was the donor age and cause of death for each sample. Any additional diseases that could affect the normal morphology of the lens capsule, such as Alport's syndrome or Marfan syndrome, were unknown. Therefore, we cannot say with certainty that the samples included in this study are accurate representatives of their respective age group. Because of this, the conclusions that can be made in this study are limited.

The results suggest that the fractal method, in correlation with stereometric and fractal analysis, provided a correct description for the three-dimensional surface of the human lens capsule. Inclusion of the fractal dimension provided additional insight into surface structure and roughness. Further investigation of these parameters as a function of age or disease state would help determine the utility of the fractal dimension as a morphometric biomarker.

This study successfully characterized the three-dimensional ultrastructural details of the surface of the anterior human lens capsule as a function of age. Novel fractal analysis techniques were applied to this structure. The results of the fractal analysis correlated with the MFP-3D analysis of the AFM data, but they provided greater insight into subtle ultrastructural changes that could occur during human lenses' disease evolution. Significant changes in the three-dimensional surface microtexture of the anterior human lens capsule were found with age, although more experiments on a larger dataset are needed to conclude this with certainty. The anterior surface of the lens capsule is complex in character, and these subtle changes in the fractal parameters observed with age may have important implications in its overall physiology. Structural changes may affect its ability to maintain the inner lens material, distribute forces during accommodation, or act as a semipermeable membrane for chemical exchange. Thus, fractal analysis may represent a valid biomarker for quantifying ultrastructural changes in the early stages of disease and help predict the disease evolution.

REFERENCES

1. Fisher RF. The structure and function of basement membrane (lens capsule) in relation to diabetes and cataract. Trans Ophthalmol Soc U K 1985; 104:755-9. .

2. Danysh BP, Czymmek KJ, Olurin PT, Sivak JG, Duncan MK. Contributions of mouse genetic background and age on anterior lens capsule thickness. Anat Rec 2008; 291:1619-27. [PMID: 18951502].

3. Danysh BP, Patel TP, Czymmek KJ, Edwards DA, Wang L, Pande J, Duncan MK. Characterizing molecular diffusion in the lens capsule. Matrix Biol 2010; 29:228-36. .

4. Danysh BP, Duncan MK. The lens capsule. Exp Eye Res 2009; 88:151-64. [PMID: 18773892].

5. Barnard K, Burgess SA, Carter DA, Woolley DM. Three-dimensional structure of type IV collagen in the mammalian lens capsule. J Struct Biol 1992; 108:6-13. [PMID: 1562433].

6. Doudevski I, Rostagno A, Cowman M, Liebmann J, Ritch R, Ghiso J. Clusterin and complement activation in exfoliation glaucoma. Invest Ophthalmol Vis Sci 2014; 55:2491-9. [PMID: 24550356].

7. Choi S, Lee HJ, Cheong Y, Shin JH, Jin KH, Park HK, Park YG. AFM study for morphological characteristics and biomechanical properties of human cataract anterior lens capsules. Scanning 2012; 34:247-56. [PMID: 22331648].

8. Creasey R, Sharma S, Craig JE, Gibson CT, Ebner A, Hinterdorfer P, Voelcker NH. Detecting protein aggregates on untreated human tissue samples by atomic force microscopy recognition imaging. Biophys J 2010; 99:1660-7. [PMID: 20816080].

9. Tsaousis KT, Karagiannidis PG, Kopsachilis N, Symeonidis C, Tsinopoulos IT, Karagkiozaki V, Lamprogiannis LP, Logothetidis S. Measurements of elastic modulus for human anterior lens capsule with atomic force microscopy: the effect of loading force. Int Ophthalmol 2014; 34:519-23. [PMID: 24037592].

10. Sueiras VM, Moy VT, Ziebarth NM. Lens capsule structure assessed with atomic force microscopy. Mol Vis 2015; 21:316-23. [PMID: 25814829].

11. Binnig G, Quate CF, Gerber C. Atomic force microscope. Phys Rev Lett 1986; 56:930-[PMID: 10033323].

12. Talu S. Mathematical methods used in monofractal and multifractal analysis for the processing of biological and medical data and images. Anim Biol Anim Husb 2012; 4:1-4. .

13. Talu S. Texture analysis methods for the characterisation of biological and medical images. Extreme Life Biospeol Astrobiol 2012; 4:8-12. .

14. Talu S. Micro and nanoscale characterization of three dimensional surfaces. Basics and applications. Cluj-Napoca, Romania: Napoca Star Publishing House; 2015.

15. Talu S. Characterization of retinal vessel networks in human retinal imagery using quantitative descriptors. Human & Veterinary Medicine 2013; 5:52-7. .

16. Talu S. Multifractal geometry in analysis and processing of digital retinal photographs for early diagnosis of human diabetic macular edema. Curr Eye Res 2013; 38:781-92. [PMID: 23537336].

17. Talu S, Stach S. Multifractal characterization of unworn hydrogel contact lens surfaces. Polym Eng Sci 2014; 54:1066-80. .

18. Talu S, Stach S, Sueiras V, Ziebarth NM. Fractal analysis of AFM images of the surface of Bowman's membrane of the human cornea. Ann Biomed Eng 2015; 43:906-16. [PMID: 25266935].

19. Talu SGS. Fractal and multifractal analysis of human retinal vascular network: a review. Human & Veterinary Medicine 2011; 3:205-12. .

20. Augusteyn RC, Rosen AM, Borja D, Ziebarth NM, Parel JM. Biometry of primate lenses during immersion in preservation media. Mol Vis 2006; 12:740-7. [PMID: 16865087].

21. Cammarata PR, Cantu-Crouch D, Oakford L, Morrill A. Macromolecular organization of bovine lens capsule. Tissue Cell 1986; 18:83-97. [PMID: 3515629].

22. Cammarata PR, Spiro RG. Identification of noncollagenous components of calf lens capsule: evaluation of their adhesion-promoting activity. J Cell Physiol 1985; 125:393-402. [PMID: 3905828].

23. Kohno T, Sorgente N, Ishibashi T, Goodnight R, Ryan SJ. Immunofluorescent studies of fibronectin and laminin in the human eye. Invest Ophthalmol Vis Sci 1987; 28:506-14. [PMID: 3549611].

24. Muraoka M, Hayashi T. Three polypeptides with distinct biochemical properties are major alpha chain-size components of type IV collagen in bovine lens capsule. J Biochem 1993; 114:358-62. [PMID: 8282726].

25. Parmigiani C, McAvoy J. Localisation of laminin and fibronectin during rat lens morphogenesis. Differentiation 1984; 28:53-61. .

26. Brinker JM, Pegg MT, Howard PS, Kefalides NA. Immunochemical characterization of type IV procollagen from anterior lens capsule. Coll Relat Res 1985; 5:233-44. [PMID: 2412754].

27. Kelley PB, Sado Y, Duncan MK. Collagen IV in the developing lens capsule. Matrix Biol 2002; 21:415-23. [PMID: 12225806].

28. Dong L, Chen Y, Lewis M, Hsieh JC, Reing J, Chaillet JR, Howell CY, Melhem M, Inoue S, Kuszak JR, DeGeest K, Chung AE. Neurologic defects and selective disruption of basement membranes in mice lacking entactin-1/nidogen-1. Lab Invest 2002; 82:1617-30. [PMID: 12480912].

29. Laurent M, Lonchampt MO, Regnault F, Tassin J, Courtois Y. Biochemical, ultrastructural and immunological study of in vitro production of collagen by bovine lens epithelial cells in culture. Exp Cell Res 1978; 115:127-42. [PMID: 210028].

30. Rossi M, Morita H, Sormunen R, Airenne S, Kreivi M, Wang L, Fukai N, Olsen BR, Tryggvason K, Soininen R. Heparan sulfate chains of perlecan are indispensable in the lens capsule but not in the kidney. EMBO J 2003; 22:236-45. [PMID: 12514129].

31. Peterson PE, Pow CS, Wilson DB, Hendrickx AG. Localisation of glycoproteins and glycosaminoglycans during early eye development in the macaque. J Anat 1995; 186:31-42. [PMID: 7649817].

32. Fukai N, Eklund L, Marneros AG, Oh SP, Keene DR, Tamarkin L, Niemela M, Ilves M, Li E, Pihlajaniemi T, Olsen BR. Lack of collagen XVIII/endostatin results in eye abnormalities. EMBO J 2002; 21:1535-44. [PMID: 11927538].

33. Ylikarppa R, Eklund L, Sormunen R, Muona A, Fukai N, Olsen BR, Pihlajaniemi T. Double knockout mice reveal a lack of major functional compensation between collagens XV and XVIII. Matrix Biol 2003; 22:443-8. [PMID: 14614990].

34. Fuerst PG, Rauch SM, Burgess RW. Defects in eye development in transgenic mice overexpressing the heparan sulfate proteoglycan agrin. Dev Biol 2007; 303:165-80. [PMID: 17196957].

35. Truscott RJ. Age-related nuclear cataract-oxidation is the key. Exp Eye Res 2005; 80:709-25. [PMID: 15862178].

36. Truscott RJW, Augusteyn RC. Oxidative Changes in Human Lens Proteins during Senile Nuclear Cataract Formation. Biochim Biophys Acta 1977; 492:43-52. [PMID: 861252].

37. Truscott RJ, Friedrich MG. Old proteins and the Achilles heel of mass spectrometry. The role of proteomics in the etiology of human cataract. Proteomics Clin Appl 2014; 8:195-203. [PMID: 24458544].

38. Truscott RJ, Zhu X. Presbyopia and cataract: a question of heat and time. Prog Retin Eye Res 2010; 29:487-99. [PMID: 20472092].

39. Shi Y, Tu Y, De Maria A, Mecham RP, Bassnett S. Development, composition, and structural arrangements of the ciliary zonule of the mouse. Invest Ophthalmol Vis Sci 2013; 54:2504-15. [PMID: 23493297].

40. Hiraoka M, Inoue K, Ohtaka-Maruyama C, Ohsako S, Kojima N, Senoo H, Takada M. Intracapsular organization of ciliary zonules in monkey eyes. Anat Rec 2010; 293:1797-804. [PMID: 20652933].

Articles are provided courtesy of Emory University and the Zhongshan Ophthalmic Center, Sun Yat-sen University, P.R. China. The print version of this article was created on 31 December 2018. This reflects all typographical corrections and errata to the article through that date. Details of any changes may be found in the online version of the article.